Contract No.:

This manuscript has been authored by Savannah River Nuclear Solutions (SRNS), LLC under Contract No. DE-AC09-08SR22470 with the U.S. Department of Energy (DOE) Office of Environmental Management (EM).

Sequestration of U(VI) from Acidic, Alkaline and High Ion-Strength Aqueous Media by Functionalized Magnetic Mesoporous Silica Nanoparticles: Capacity and Binding Mechanisms

Dien Li[‖,*], Shani Egodawatte[‡], Daniel I. Kaplan[‖], Sarah C. Larsen[‡], Steven M. Serkiz[‖], John C. Seaman[¶], Kirk G. Scheckel[†], Jinru Lin[§], Yuanming Pan[§]

[‖] Savannah River National Laboratory, Aiken, SC 29808, USA

[‡] Department of Chemistry, University of Iowa, Iowa City, IA 52242, USA

[¶] Savannah River Ecology Laboratory, University of Georgia, Aiken, SC 29802, USA

[†] U.S. Environmental Protection Agency, National Risk Management Research Laboratory, Cincinnati, Ohio 45224, USA

[§] Department of Geological Sciences, University of Saskatchewan, Saskatoon, SK S7N 5A5, Canada

ABSTRACT: Uranium(VI) exhibits little adsorption onto sediment minerals in acidic, alkaline or high ion-strength aqueous media that often occur in U mining or contaminated sites, which makes U(VI) very mobile and difficult to sequester. In this work, magnetic mesoporous silica nanoparticles (MMSNs) were functionalized with several organic ligands. The functionalized MMSNs were highly effective and had large binding capacity for U sequestration from high salt water (HSW) simulant (54 mg U/g sorbent). The functionalized MMSNs, after U exposure in HSW simulant, pH 3.5 and 9.6 artificial groundwater (AGW), were characterized by a host of

spectroscopic methods. Among the key novel findings in this work was that in the HSW simulant or high pH AGW, the dominant U species bound to the functionalized MMSNs were uranyl or uranyl hydroxide, rather than uranyl carbonates as expected. The surface functional groups appear to be out-competing the carbonate ligands associated with the aqueous U species. The uranyl-like species were bound with N ligand as η^2 bound motifs or phosphonate ligand as a monodentate, as well as on tetrahedral Si sites as an edge-sharing bidentate. The N and phosphonate ligand-functionalized MMSNs hold promise as effective sorbents for sequestering U from acidic, alkaline or high ion-strength contaminated aqueous media.

TOC for abstract

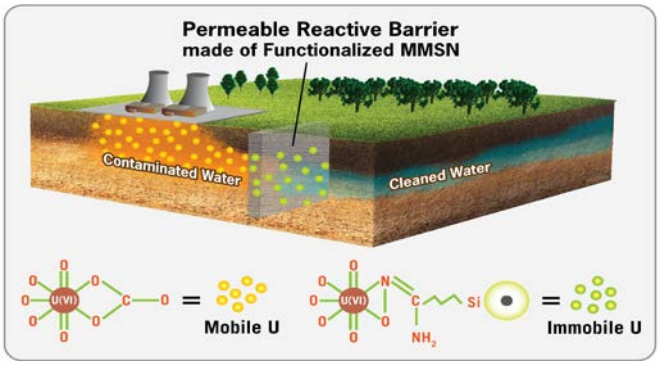

KEYWORDS: Uranium, Aqueous media, Nanoparticle sorbents, Capacity, binding chemistry

1. INTRODUCTION

Uranium contamination often occurs in acidic (e.g., Savannah River Site F-area, pH = 3-4)[1] or alkaline (e.g., the Hanford Site 300 area, pH = 8-9)[2] groundwater or high ion-strength aqueous media (e.g., U mine and industrial wastes)[3]. In such aqueous media under oxic condition, U(VI) species (e.g., UO_2^{2+} and UO_2^{2+}-carbonate) typically exhibit weak adsorption to sediments, which leads to its high environmental mobility and difficult sequestration. One of the favored

remediation strategies for U is the reduction of U(VI) to its less mobile form U(IV). For example, microbial reduction[4] and zero-valent iron[5] have been effective in decreasing the risk associated with U contamination to the environment. However, bioreduction technologies need to inject electron donors (e.g., acetate and ethanol) to stimulate the microorganism population for its sustainable effectiveness, while chemical reduction approaches are not applicable to the low pH systems. More importantly, the reductive product, U(IV) dioxide, is readily re-oxidized and U(VI) is re-mobilized under most of the environmental conditions.[6-8] Thus, there is a great need to develop more robust technologies for remediation of U from acidic, alkaline and high ion-strength contaminated systems.

In addition, the U concentration in seawater is ~3.3 μg/L, with a total global pool of ~4.3 billion tons of U in seawater,[9] which can support nuclear power production at the current capacity for nearly 72,000 years. However, an extraordinary challenge for extracting U from seawater of high salt and complex aqueous chemistry is to develop efficient and cost-competitive recovery technologies.[10, 11] Over the last six decades, the majority of such research activities have focused on inorganic materials (e.g., hydrous titanium oxide),[12] chelating polymers (e.g., amidoxime-based polymers),[10, 13] nanomaterials (e.g., mesoporous carbon[14, 15] and silica[16-18]), and biologically derived sorbents.[19] Amidoxime-based resins or nanomaterials have been demonstrated to be the most promising adsorbents for recovering U from seawater.[10] While considerable progress has been achieved, the current state-of-the-art adsorbents nevertheless suffer from severe deficiency in appropriate species selectivity. Therefore, selective and cost-effective adsorbent materials that can lead to feasible and economical technologies for extracting U from seawater remain an important research need.

Aqueous U speciation is unusually complex because it readily undergoes hydrolysis, is redox sensitive, and forms numerous strong complexes especially to environmental concentrations of phosphate, Cl^-, natural organic matter, carbonate, calcium and magnesium.[20-23] Furthermore, pH not only has an impact on the extent of hydrolysis, but also influences the types of complexes, the extent of (co)precipitation, type of complexes that form, and the extent that polyatomic species are formed. Uranium speciation has been shown to greatly impact sorption to mineral surfaces. More specifically, in the Ca-Mg-carbonate aqueous systems, the formation constant calculations demonstrated that $CaUO_2(CO_3)_3^{2-}$ is more important than $Ca_2UO_2(CO_3)_3$ and that the $Ca_2UO_2(CO_3)_3$ distribution increased with increasing Ca^{2+} concentration. Uranium sorption onto anion-exchange resins is inhibited by the formation of the neutral $Ca_2UO_2(CO_3)_3^0$ species.[24]

In this work, we developed magnetic mesoporous silica nanoparticles (MMSNs) that were further grafted with dihydroimidazole (DIM), polyacryloamidoxime (AD), phosphonate (PP), phosphonate-amino (PPA), poly(propylenimine) dendrimer (PPI), and poly(amidoamine) dendrimer (PM). The new functionalized MMSNs are magnetic for the purpose of easy post-use retrieval, possess high surface areas and mesopore structures to provide more active binding sites and greater accessibility, with organic binding ligands that can selectively retain U and improve adsorption capacity. The objectives of this work were as follows:1) evaluate the adsorption capacities using batch adsorption experiments of these functionalized MMSNs for removing U from three model systems: high salt water (HSW) simulant, low pH artificial groundwater (AGW) and high pH AGW; 2) identify the U speciation sorbed to the functionalized MMSNs using U L_3-edge synchrotron X-ray absorption near structure (XANES), Fourier transform infrared (FTIR) and electron paramagnetic resonance (EPR) spectroscopies; and 3) elucidate the molecular mechanisms responsible for U species binding to the functionalized MMSNs surfaces

using U L_3-edge extended X-ray absorption fine structure (EXAFS) spectroscopy. One of the key novel findings in this work is that the dominant U species bound to the most effective sorbents were uranyl or uranyl hydroxide, rather than the expected uranyl carbonate species. It is further postulated that the surface functional groups of the MMSNs out-competed the carbonate ligands associated with the aqueous U species.

2. MATERIALS AND METHODS

2.1. Materials. 3-Aminopropyltriethoxysilane, acrylonitrile, hydroxylammonium chloride (NH_2OH•HCl), 3-(trihydroxysilyl)propyl methylphosphonate, (3-chloropropyl)triethoxysilane, polyamidoamine dendrimers, polypropylenimine dendrimers, tetraethoxysilane, hexadecyltrimethyl-ammonium bromide, 1,4-dioxane, were purchased from Sigma Aldrich. Nitric acid, sodium hydroxide, dichloromethane, and diethyl ether were purchased from Fisher Scientific. N-(3-triethoxysilylpropyl)-4,5-dihydroimidazole and diethylphosphato-ethyltriethoxysilane were purchased from Gelest, boric acid (99.8%) was purchased from Alfa Aeser, and hydrofluoric acid (51% in water) was purchased from Acros Organics. All chemicals were used as received.

2.2. Synthesis of MMSNs. The magnetite nanoparticles were synthesized under argon condition based on a slight modification of a published one-pot chemical co-precipitation method.[25] Typically, they were spherical in shape and had a particle size of ~11 nm.[25] MMSNs were synthesized using a surfactant template method that has been described in literature.[25-27] In this approach (Figure 1A), hexadecyltrimethyl-ammonium bromide (1 g), NaOH (3.5 mL, 2M), and water (500 mL) were mixed with Fe_3O_4 nanoparticles (300 mg) and sonicated. The contents were heated at 80 °C and tetraethoxysilane was added. The reaction mixture was aged for 2 h and

111 then filtered, washed with deionized water and methanol, and dried at 120 °C overnight. The
112 surfactant template was removed by calcining the product at 600 °C for 6 h to obtain MMSNs.
113 After calcilation, the magnetite core might partially or completely be transformed to
114 maghemite.[25] The Fe content of the MMSNs was 13 wt%.[26] The superparamagnetism of the
115 MMSNs was demonstrated, but its magnetic property was considerably lower than the magnetite,
116 due to the reduced weight percentage of magnetite in MMSNs.[25] In addition to facilitating easy
117 removal of the nanoparticles from the solution phase, we examined whether the magnetite core
118 would enhance the adsorption of U. However, our initial studies showed that the magnetic and
119 the non-magnetic mesoporous silica nanoparticles showed similar adsorption capacities for
120 uranium. As a result, we focused our study on magnetic MMSNs.
121 2.3. Functionalization of MMSNs with organic molecules. Functionalization of MMSNs with
122 dihydroimidazole group,[28] polyacryloamidoxime group,[29] phosphonate group,[16] phosphonate-
123 amino group,[30] poly(propylenimine) dendrimer group,[31] and poly(amidoamine) dendrimer
124 group[31] was conducted using a post synthesis method through a silane coupling group that is
125 bonded with mesoporous silica surfaces.[26] The details for surface functionalization were
126 described in Supporting Information (SI), and the structures of the functionalized molecules were
127 displayed in SI Figure S1. Briefly, as shown in Figure 1B, calcined MMSNs (1 g) were refluxed
128 with a certain amount of chosen organic molecules in solvents (toluene or 1,4-dioxane) at 120 °C
129 for 6 h. The reaction mixture was filtered and washed with a 1:1 mixture of diethylether and
130 dichloromethane, or methanol, and then dried overnight at 100 °C. However, for
131 polyacryloamidoxime group functionalization, aminopropyl functionalized MMSNs (1 g) were
132 refluxed with acrylonitrile (8 mmol) in methanol at 65 °C for 12 h under N_2 atmosphere. The
133 reaction mixture was filtered and washed with 1:1 mixture of diethyl ether and dichloromethane,

and then dried at 50 °C overnight in an oven. The product obtained from the above reaction was then mixed with 0.5 g of NH_2OH•HCl and 50 ml of methanol. The pH of the reaction mixture was adjusted to 8 and it was equilibrated at 70 °C for 24 h. The reaction mixture was filtered, washed with methanol and then dried at 50 °C overnight.[29] In addition, phosphonate-amino functionalized MMSNs were made using 3-aminopropyltriethoxysilane and diethylphosphato-ethyltriethoxysilane refluxion in toluene, while poly(propylenimine) and poly(amidoamine) dendrimer group functionalization was conducted after pre-functionalization of MMSNs with chloropropyl group.[31] The physical and chemical properties of the functionalized MMSNs are characterized using the N_2 adsorption-desorption isotherms (SI Figure S2), small and high angle powder X-ray diffraction (SI Figure S3), thermogravimetric analysis, transmission electron microscopy (SI Figure S4), ^{13}C cross-polarisation magic angle spinning solid state nuclear magnetic resonance spectroscopy (SI Figure S5).[26] The considerable difference in the saturation magnetization of the amine functionalized and non-functionalized MMSNs also suggested that the functionalization further decrease the magnetic property of the functionalized MMSNs.[25]

2.4. Batch experiments for U adsorption isotherms. Batch U(VI) sorption experiments for obtaining the adsorption isotherms (the mass of U sorbed onto the sorbent (q_e, mg/g) versus solution U concentration at equilibrium) were conducted in pH 8.1 HSW simulant under ambient atmospheric CO_2 and temperature (22 °C). The HSW simulant was made following literature protocol[32] and this specific HSW recipe was selected in order to evaluate the functionalized MMSNs for U removal from both high ion-strength aqueous media like contaminated water and seawater. The nominal chemical composition of the HSW simulant (in mg/L) was Na 10,760, K 390, Mg 1,280, Ca 410, Cl 19,380, SO_4 2,910, and CO_3 140. For each set of experiments, a sorbent-free control was included as the initial U concentration for adsorption quantity (q_e)

calculations and to provide an indication of U sorption to labware during the experiment. Approximately 0.0075 or 0.0040 g MMSNs and 7.1 to 7.5 mL HSW simulant were added to 15 mL polypropylene centrifuge tubes prior to U spiking. Uranyl nitrate hexahydrate (^{238}U, Electron Microscopy Sciences, Hatfield, PA) was used to make the U stock solution (5×10^{-3} M, pH 3.6, and Eh 433 mV). After spiking with 0.0375 mL to 0.375 mL of the U stock solution, an initial U concentration of 2.5×10^{-5} M (6 ppm) to 2.5×10^{-4} M (59.5 ppm) in the working solution was targeted. The great initial U concentrations were used in this study to evaluate the adsorption capacity of the functionalized MMSNs and to prepare samples with reasonably high U loading for spectroscopic measurements. The suspensions were adjusted to pH 8.1 with 1 M NaOH or 1 M HNO_3, and equilibrated on a reciprocating shaker for 6 days. The solution pH values were also adjusted daily until the change in pH was < 0.1 pH unit (Radiometer Copenhagen PHM 95 pH meter). After equilibration for 6 days, each suspension was filtered using 0.2 μm pore size nylon membrane syringe filters. The filtrate was acidified with 2% HNO_3 in a typical 1:10 ratio and analyzed for U by inductively coupled plasma mass spectrometry (ICP-MS; NexION 300X, Perkin Elmer, Inc.). The ICP-MS analyses had an uncertainty of ± 10%, but our repeatability test indicated that this uncertainty was often within ± 5%. The solid samples were air dried and collected for spectroscopic characterization.

Similarly, batch experiments were conducted to obtain functionalized MMSN samples with U exposure in pH 3.5 and 9.6 AGW for U speciation and chemical binding studies by spectroscopic measurements. The AGW was prepared following a literature protocol,[1] and its nominal composition (in mg/L) was Na 1.25, K 0.25, Ca 0.93, Mg 0.66, Cl 5.51, and SO_4 0.73. During equilibration, all tubes were open to the lab atmosphere without shaking twice per day for 1 h to promote equilibration with atmospheric CO_2, and the suspension pH values were adjusted

daily until it was < 0.1 pH unit within the target of 3.5 or 9.6.[26] The nominal U loadings in these samples varied, up to 9000 ppm, based on U adsorption percentages from the batch experiment.

2.5. FTIR and EPR measurements. Samples for FTIR measurements were prepared by mixing the air-dried sample with KBr. FTIR spectra were obtained at room temperature with a Bio-RAD FTS-40 instrument under the reflectance mode, in the range from 4400 to 400 cm^{-1} and a spectral resolution of 2 cm^{-1}. An average of 265 scans were made and corrected against a background spectrum of KBr. Samples for EPR measurements were irradiated in a ^{60}Co cell (dose rate of ~460 Gy/h) for 2 days and were mixed with KBr for dilution. EPR spectra were measured at room temperature on a Bruker EMX spectrometer, operated at microwave frequencies of ~9.73 GHz, a modulation frequency of 100 kHz, a modulation amplitude of 0.1 mT, microwave powers of 0.2 mW and 6.35 mW, and a spectral resolution of 0.01 mT.

2.6. U L_3-edge XANES / EXAFS measurement and data analysis. After U adsorption, U L_3-edge XANES and EXAFS spectra of all functionalized and reacted MMSNs were collected using the Materials Research Collaborative Access Team (MRCAT) Sector 10-ID beamline at the Advanced Photon Source (APS) (Argonne National Lab, Argonne, IL). Experimentally, 50-100 mg of each of the air-dried powder samples was pressed into a 6.3-mm diameter disk and sealed in Kapton tape double containment. The MRCAT Sector 10-ID beam line used a double crystal water cooled Si (111) monochromator, detuned to 50% of peak intensity to minimize higher order harmonics.[33] The APS storage ring was operated at 100 ± 5 mA during the measurements. The monochromator was calibrated to 17038 eV using the first inflection point of the K-edge of yttrium metal foil, and the foil was recorded for all samples scans utilizing a reference ion chamber. The U L_3-edge XANES and EXAFS spectra were collected in 20 scans using

fluorescence step-scanning mode with a Vortex 4-element silicon drift diode over the energy range of 17000-17750 eV at room temperature.

All the collected spectra were processed and analyzed using the IFEFFIT software package including Athena and Artemis.[34, 35] Data from multiple scans were processed using Athena by aligning and merging the spectra followed by background subtraction using the AUTOBK algorithm. The U L_3-edge EXAFS data analysis were conducted on the merged and normalized spectra using Artemis.[36] UO_2(benzamidoximate)$_2$($MeOH$)$_2$ (U=O_{ax}, U-O_{eq}, U-N, and U=O_{ax} multiple scattering paths),[37] chernikovite ((H_3O)(UO_2)(PO_4)·3(H_2O)) (U-P path)[38] and soddyite (U-Si path)[39] were used as reference structural models. Fits to the EXAFS data were made in R space (R from 1.2 to 4.0 Å) and obtained by taking the Fourier transform (FT) of χ(k) (k from 3 to 10.2) with a k weighting of 2. Although reasonably good signal-to-noise ratio oscillations at more distant k up to 13 were obtained, the FT of χ(k) was taken at k from 3 to 10.2, because there was a glitch at k ~10.5.

3. RESULTS AND DISCUSSION

3.1. Capacities of functionalized MMSNs for U sequestration.

Uranium exists primarily as uranyl (UO_2^{2+}) in pH 3.5 AGW and as uranyl carbonate species (e.g., $UO_2(CO_3)_3^{4-}$ and $UO_2(CO_3)_2^{2-}$) in HSW simulant and pH 9.6 AGW (SI Figure S6). These species display limited adsorption to common sediment minerals and synthetic sorbents in the corresponding aqueous media, primarily due to electrostatic repulsion of ionic species, steric hindrance from the enlarged molecular radius, and difficulty in displacement of the strongly bound CO_3^{2-} species.[40] Functionalization of MMSNs with selected organic ligands enhances U species binding to the

ligands and our strategy was to use this phenomenon to engineer high affinity binding sites for U adsorption. In order to evaluate the performance of the functionalized MMSNs for U removal, the mass of U adsorbed onto the sorbent (q_e, mg/g) was calculated based on batch experimental data (equation 1):

$$q_e = \frac{(C_0 - C_e) \times V}{M} \quad (1)$$

where C_0 (mg/L) is the initial U concentration in the control samples, C_e (mg/L) is U concentration in the solution at equilibrium, V is the volume of the solution (L) and M is the mass of the sorbent (g).

The adsorption isotherms of U onto the functionalized MMSNs in the HSW simulant are shown graphically in Figure 2A. These isotherm data were fitted using the Langmuir isotherm model (equation 2).

$$\frac{C_e}{q_e} = \frac{1}{q_{max}} C_e + \frac{1}{K_L q_{max}} \quad (2)$$

where q_e is the mass of U adsorbed onto the sorbent at equilibrium (mg/g), q_{max} is the saturation sorption capacity (mg/g), C_e is the U(VI) concentration in solution at equilibrium (mg/L), and K_L is the Langmuir constant that is directly related to the binding site affinity (L/mg).

Representative Langmuir fits of equilibrium data for U adsorption onto dihydroimidazole-functionalized MMSNs, MMSNs-PP, and MMSNs-PPI are shown in Figure 2B. The q_{max} (mg/g) and the associated coefficient of correlation (R^2) that provides a measure of the model fit to the experimental data were obtained by plotting C_e/q_e versus Ce. The q_{max} values of these functionalized MMSNs for U sequestration from the HSW simulant are summarized in Table 1, and for the purpose of comparison, previously reported q_{max} values of U removal from pH 3.5 and 9.6 AGW are also presented.[26] The q_{max} values of all functionalized MMSNs for U

sequestration from the HSW simulant were 34-54 mg/g, with MMSNs-PM having the highest adsorption capacity. In comparison, the q_{max} values of the functionalized MMSNs for U removal from the pH 3.5 and 9.6 AGW were as high as 38 and 133 mg/g, respectively, The fits obtained from the Langmuir model had a significant correlation coefficient ($R^2 > 0.93$), indicating that the model generally described the sorption data well (Table 1). However, sorption plateaus indicative of limited capacity were not completely achieved for all sorbent isotherms, and the calculated saturation capacities may likely provide lower estimates than those that may actually exist. In addition, although the adsorption capacity of U on non-functionalized MMSNs in the HSW simulant was not determined, its adsorption K_d value was ~7800 mL/g, but smaller than the K_d values for the functionalized MMSNs (SI Figure S7). These results indicated that in the very HSW simulant, U can be adsorbed on the non-functionalized MMSNs, but the organic functionalization further improved its adsorption capacity.

The adsorption capacities for some relevant materials (e.g., organo-functionalized mesoporous silica, and amidoxime polyethylene fibers) for U extraction from seawater have been reported in recent literature. The U adsorption capacities of polyacryloamidoxime (46 mg/g) and phosphonate (45 mg/g) functionalized MMSNs from the HSW simulant are fairly comparable to functionalized mesoporous silica reported in recent literature (i.e., 30-57 mg/g for amidoxime-modified mesoporous silica,[18] 11-54 mg/g for phosphonic mesoporous silica,[17] and 21-66 mg/g for a host of other organo-functionalized mesoporous silica[16]). For a direct comparison, the current work demonstrated that poly(propylenimine) (52 mg/g) and poly(amidoamine) dendrimer (54 mg/g) functionalized MMSNs had slightly higher adsorption capacities than those of polyacryloamidoxime and phosphonate functionalized MMSNs. Radiation-induced graft polymerization of acrylonitrile onto high surface area polyethylene

fibers can significantly improve the degree of grafting by up to 350%.[41] With conditioning in 0.44 M KOH at 80 °C, the new amidoxime-polymer adsorbents are very effective in U extraction from seawater simulant with 6 ppm U with reported capacities of 170-200 mg/g, although the U capacity of the same adsorbent decreased to 3-5 mg/g when tested with natural seawater.[41] Therefore, U concentration effect, the uranyl to bicarbonate ratio, and the presence of calcium and other competing ions in the tested aqueous media may dramatically impact uranium adsorption capacity. As a result, the capacity data obtained from different experimental setup may not directly be comparable. However, the high surface area mesoporous silica appears to be a generally more effective matrix than mesoporous carbon[14] and typical polyethylene polymer matrix for U sequestration from HSW.[10]

For environmental remediation applications, for example, as an additive remedy in permeable reactive barrier, the reuse of the adsorbents may not be critical. However, it is important to evaluate the regeneration and reuse of these adsorbents for U removal, especially for the potential applications in U mining from seawater. The ~90% of the adsorbed U on these adsorbents could be desorbed by using 0.5 M nitric acid (our unpublished data). Although these adsorbents were not evaluated for several adsorption-desorption cycles, by referring to a previous study,[42] the adsorption capacity of a similar amidoxime-functionalized magnetic mesoporous silica for U removal from pH 5.0 aqueous solution was demonstrated to decrease by only ~6% after five adsorption-desorption cycles. Thus, it is expected that these adsorbents reported in this study can remain fairly effective for U removal after several adsorption-desorption cycles.

3.2. Uranium speciation. The U L_3-edge XANES spectra of the functionalized MMSNs after exposure to U in the HSW simulant are shown in Figure 3, in comparison with the standard

spectra of uraninite ($U(IV)O_2$), uranyl phosphate ($Ca(UO_2)_2(PO_4)_2 \cdot 10\text{-}12H_2O$), uranyl carbonate ($UO_2(CO_3)$), uranyl nitrate ($UO_2(NO_3)_2 \cdot 6H_2O$), and schoepite ($((UO_2)_8O_2(OH)_{12} \cdot 12H_2O$), while the spectra of the functionalized MMSNs with U adsorption from pH 3.5 and 9.6 AGW are shown in SI Figure S8. Graphic comparison and linear combination fitting all indicated that the adsorbed U species on these functionalized MMSNs from the three aqueous media was U(VI), rather reduced U(IV). This should not be surprising, because of the chemistry of organic ligands (amines or phosphonate) used. However, the U L_3-edge XANES data cannot conclusively identify whether the adsorbed U(VI) species was uranyl or the most dominant uranyl carbonate (i.e., $UO_2(CO_3)_3^{4-}$ and $UO_2(CO_3)_2^{2-}$) in the HSW simulant or pH 9.6 AGW (SI Figure S8). One exception was phosphonate functionalized MMSNs retrieved from the pH 3.5 AGW adsorption experiment. Its U L_3-edge XANES spectrum, even in the very first scan, indicated that the dominant U species was U(IV) (SI Figure S8). This result was not understood yet, it might be related to the presence of functional phosphonate, which might make the U species more prone to radiation reduction or facilitate the formation of monomer U(IV) species.[43] However, this warrants a future investigation.

The same six functionalized MMSN samples retrieved from the HSW simulant were further analyzed by FTIR and EPR to determine whether a carbonate species was present. These samples had nominal U concentrations up to 9,000 ppm, as calculated from U adsorption experiments. The FTIR spectra of these samples and polyacryloamidoxime functionalized MMSNs without U adsorption are shown in Figure 4A. A small band at ~900 cm^{-1} for the samples dihydroimidazole, polyacryloamidoxime, phosphonate and phosphonate-amino functionalized MMSNs is suggestive of the presence of detectable uranyl. However, the

symmetric vibrational band at ~1360 cm^{-1} and the asymmetric vibrational band at ~1500 cm^{-1} for CO_3^{2-} are absent in these spectra,[44] indicating no detectable carbonate in these samples.

The EPR spectra of all six samples after gamma-ray irradiation are characterized by broad resonance signals centered at the g_{eff} value of ~2.20 (Figure 4B), which arise from superparamagnetism of magnetite nanoparticles.[45, 46] A weak resonance signal at g = ~2.00 is also observed in all samples investigated in this study (Figure 4B). The EPR spectra of polyacryloamidoxime (AD) functionalized MMSNs without U exposure before and after gamma irradiation were also included in the inset of Figure 4B for comparison. The g = ~2.00 signal was absent for the non-irradiated sample, but present for the gamma-irradiated sample. The spectra simulation demonstrated that this g = ~2.00 signal was arisen from the irradiated induced E' center in silica.[47] Thus, this signal at g = ~2.00 for all functionalized MMSNs exposed to U is attributable to radiation-induced E' center in silica, and it can be ruled out as any known carbonate-related radicals (i.e., CO_2^-, CO_3^{3-} and CO_3^- formed from the diamagnetic precursor CO_3^{2-}) on the basis of spectral simulations.[48, 49] The EPR technique is well known for its superior sensitivity over other spectroscopic methods such as FTIR for the detection and characterization of dilute paramagnetic species in the bulk or on the surfaces.[50] Therefore, these EPR data provide another line of compelling evidence for the absence of carbonate in our samples under the described experimental conditions.

Dominant U species in carbonate-containing aqueous systems like HSW simulant and pH 9.6 AGW are uranyl carbonate species (i.e., $UO_2(CO_3)_3^{4-}$ and $UO_2(CO_3)_2^{2-}$) (SI Figure S6). However, the speciation of the adsorbed U species from carbonate aqueous media remains unresolved. U(VI)-carbonate species were identified as edge-sharing bidentate complexes onto calcite-water interface at pH 7.4-8.3 and under atmospheric conditions,[51] bone apatite materials

in artificial groundwater in the presence of dissolved carbonate (4.8 mM total),[52] hematite surfaces throughout the pH range of 4.7-8.2 under conditions relevant to aquifers,[44] and $Fe(O,OH)_6$ octahedral sites of chlorite present in pH 6.5-10 aqueous media containing 2.5×10^{-4} M Na_2CO_3.[53] However, sorbed uranyl carbonate species were not identified on MCM-41 in pH 9.8 aqueous media containing 0.4 mM $NaHCO_3$[54] or amidoxime-functionalized polymer fibers in seawater.[55] Gamma-ray irradiated EPR data in the current work clearly demonstrated that the U species adsorbed onto the functionalized MMSNs exposed to U in HSW simulant is a uranyl species without the carbonate group, which is further supported by U L_3-edge EXAFS data described below. Although it is not completely understood why uranyl-like species, rather than uranyl carbonates, are bound to the functionalized MMSNs in the HSW simulant, one possible scenario is that the binding ligands on the MMSNs effectively compete with carbonate for the complexation of U(VI). In fact, density functional theory calculations demonstrate that glutarimidedioxime[56] and even weaker phthalimidedioxime[57] can effectively compete with carbonate to form fairly strong U(VI) complexes under similar aqueous conditions.

3.3 Uranium binding chemistry. U L_3-edge EXAFS spectra in k-space (A), Fourier transforms plots in magnitude (B) and in the real space component (C) of the functionalized MMSNs after exposure to U in the HSW simulant are shown in Figure 5, where experimental data are shown in solid circles, and EXAFS fits are shown in color lines. The fitted EXAFS parameters of all the functionalized MMSNs are summarized in Table 2. Similarly, U L_3-edge EXAFS spectra of the functionalized MMSNs retrieved from the pH 3.5 and 9.6 AGW are shown in SI Figures S9 and S10, respectively, and the corresponding EXAFS fitting data are summarized in SI Tables S1 and S2, respectively. It is noted that the EXAFS data for phosphonate, phosphonate-amino, poly(propylenimine) dendrimer and poly(amidoamine)

dendrimer functionalized MMSNs from the pH 3.5 AGW experiments were not presented. Poly(amidoamine) dendrimer functionalized MMSNs had limited adsorption capacity in the pH 3.5 AGW, and its EXAFS was not collected. The U L_3-edge XANES of the phosphonate, phosphonate-amino and poly(propylenimine) dendrimer functionalized MMSNs displayed a significant edge shift toward lower energy by ~2 eV, starting from the respective first and second scan. Again, although the reason for this observation was unknown and warrants a future investigation, it was probably due to incident X-ray beam caused reduction. As a result, the EXAFS data fittings for these three samples were not successful. Otherwise, similar structure models were used for the EXAFS data fitting of all samples retrieved from the HSW simulant, pH 3.5 and 9.6 AGW. The following discussion focused on samples retrieved from the HSW simulant.

For dihydroimidazole, polyacryloamidoxime, poly(propylenimine) dendrimer and poly(amidoamine) dendrimer functionalized MMSNs that contain N ligands, the U L_3-edge EXAFS data were fitted with an axial oxygen path at a U-O_{ax} distance of 1.80 ± 0.01 Å with a fixed coordination number of 2, an equatorial O path at the U–O_{eq} distance of 2.25 ± 0.04 Å with a coordination number of 3.4-4.3, and an equatorial N path at the U-N distance of 2.34 ± 0.04 Å with a coordination number of 1.6-0.7. The equatorial coordination environment of this U species consists of about five light scattering atoms, which was first obtained through the U-O_{eq} path fitting and then was set to five in the subsequent fittings. Five or six equatorially coordinated atoms are common for uranyl complexes.[58] However, the identities of these light scattering atoms (e.g., N or O) cannot be directly determined by EXAFS, thus, the variations in interatomic distance and the Debye–Waller factors of the U-O_{eq} and U-N paths were set to identical values in the structure model. In addition, a U-Si path at an average distance of 3.13 ±

0.02 Å and a coordination number of 0.4-0.6 was necessarily included to fit the data to acceptable goodness of R-factor < 0.003 and reduced χ^2 < 100. The U L_3-edeg EXAFS data fittings were unsuccessful when tridentate cyclic imidioxime[59] and chelating models[55] were applied, which resulted in significant distortion of bond lengths from the crystalline models, large errors, higher R-factor and χ^2 values.

Similarly, the U L_3-edge EXAFS data of the phosphonate functionalized MMSNs was fitted with a U-O_{ax} path at an average distance of 1.81 Å with a fixed coordination number of 2, a U–O_{eq} path at a distance of 2.26 Å with a coordination number of 5.1, a U-P path at a distance of 3.56 Å and a coordination number of 0.9, and a U-Si path at a distance of 3.13 Å and a coordination number of 0.6. For phosphonate-amino functionalized MMSNs that contains both N and phosphonate ligands, the EXAFS data were fitted with the equatorial U-N path at the distance of 2.34 Å and a coordination number of 0.9, rather than the U-P path that failed in the data fitting.

For all functionalized MMSNs, U=O_{ax} multiple scattering makes an important contribution to the uranyl EXAFS and three U=O_{ax} multiple scattering paths were included to significantly improve the data fitting.[36] However, the addition of a U-C path consistently failed or deteriorated statistically in the U L_3-edge EXAFS data fitting, which tends to support that the U species adsorbed to the functionalized MMSNs in the HSW simulant are uranyl or its hydroxides, rather than uranyl carbonates, consistent with their EPR spectra.

Based on U L_3-edge EXAFS fitting data (Figure 5 and Table 2), three major uranyl binding sites were identified on the functionalized MMSNs following exposure to U in HSW simulant (Figure 6). For amidoxime-functionalized MMSNs, there are two uranyl binding sites. The first U complex is bound by N ligands with a U-N interatomic distance of 2.34 Å and varying

coordination numbers of 0.7-1.6 on the equatorial plane (Figure 6A). The coordination numbers and interatomic distances are consistent with the average local atomic environment of uranyl containing 1-2 N atoms binding in a manner similar to the η^2 motif (Figure 6A). The η^2 motif has been observed through the single-crystal X-ray diffraction studies of UO_2^{2+} complexes with acetamidoxime and benzamidoxime anions, which was used as a model in our EXAFS data fitting.[37] Recent density functional theory calculations also indicate that the η^2 binding motif is the most stable form among the evaluated possibilities, including monodentate binding to either the O or the N atom of the oxime group, bidentate chelation involving the oxime O atom and the amide N atom, and η^2 binding with the N−O bond in a series of $[UO_2(AO)_x(OH_2)_y]^{2-x}$ (x = 1−3) complexes.[37]

The second U complex on amidoxime-functionalized MMSNs is silanol bound uranyl likely as a bidentate manner with U-Si interatomic distance of 3.13 Å[60, 61] and coordination number of 0.4-0.6 (Figure 6B), which may indicate that ~50% of the total sorbed U is bound to Si sites. Although the post-synthetic functionalization of organic ligands was intended to homogeneously cover the external and internal surfaces of mesoporous silica, the degree of functionalization was optimized for achieving a balance between the amount of functional groups grafted and the surface area of the nanoparticles to make an effective adsorbent. As a result, some mesopores remained unfunctionalized or partly functionalized. The surface areas were reduced from 1010 m^2/g with a pore volume of 0.33 cm^3/g for unfurnctionalized MMSNs to ~550 m^2/g with a pore volume of ~0.11 cm^3/g for different functionalized MMSNs.[26] Uranyl species has been demonstrated to diffuse into the pore structure of mesoporous silica at a U concentration of $>1\times10^{-5}$ M.[54] Mesoporous silica was also demonstrated to have a moderately high U adsorption capacity of 7-17 mg/g from seawater,[18] in agreement with the K_d value of the non-functionalized

MMSNs (SI Figure S7). In the current study, U L_3-edge EXAFS spectrum of the unfunctionalized MMSN exposed to U in the HSW simulant also demonstrated that uranyl species are bound with Si sites in a bidentate manner. Therefore, it is not surprising that an appreciable quantity of U is bound by residual exposed Si sites of the inhomogeneously functionalized MMSNs. Nevertheless, the functionalized MMSNs displayed significantly improved U extraction capacity from the HSW simulant due to the presence of the added binding ligands when compared to the unfunctionalized mesoporous silica. The absence of any U-U scattering path in the current study support the specific binding of uranyl under our experimental conditions (i.e., high salt chemistry, U loading up to 2.5×10^{-4} M, and 6 days), and there was no polymerization of U species, as opposed to precipitation of nano-U-bearing phases inside the mesoporous silica pores at a U pore concentration of $>1\times10^{-5}$ M.[54]

For phosphonate functionalized MMSN exposed to U in the HSW simulant, the uranyl complex is bound with the phosphonate ligand as a monodentate with a U-P interatomic distance of 3.56 Å and a coordination number of 0.9 (Figure 6C). A monodentate uranyl species bound with P is also common among uranyl phosphates like chernikovite.[38] In addition, there is also the second U complex on the phosphonate functionalized MMSNs. This uranyl complex is bound with Si sites as an edge-sharing bidentate complex with a U-Si interatomic distance of 3.13 Å[60, 61] and a coordination number of 0.6 (Figure 6B), as observed for the amidoxime functionalized MMSNs. A similar interpretation of this result can be applied as provided above.

For the other N ligand (i.e., dihydroimidazole, poly(propylenimine) dendrimer and poly(amidoamine) dendrimer) functionalized MMSNs, the U L_3-edge EXAFS data were fitted using the same model applied to the amidoxime-functionalized MMSN. Similar to the data and fits discussed above, two uranyl binding sites are present: N ligands as η^2 bound-like motif and

tetrahedral Si sites as an edge-sharing bidentate surface complex. For phosphonate-amino functionalized MMSNs that contains both N and phosphonate ligands, it appears that the U L_3-edge EXAFS data was fitted well with the U-N path, similar to the other N ligand functionalized MMSNs. Data fitting failed with the U-P path, revealing limited participation in uranyl binding, which may indicate that N-based functionalities are stronger ligand than phosphonate for binding uranyl under HSW-related conditions.

3.4 Environmental Applications. Uranium contaminant exhibits little adsorption onto sediment minerals in high ion-strength, very acidic or alkaline aqueous systems that often occur in U mining or contaminated sites. As a result, U contaminant is very difficult to sequester and exerts a major risk to the environment and ecosystems. A series of six organo (i.e., amidoxime-, imidazole, phosphonate-, and dendrimer-functional groups)-functionalized magnetic mesoporous silica nanoparticles (MMSNs) were synthesized, characterized and screened for U sequestration from three model aqueous media: high salt water simulant, acidic and alkaline artificial groundwater. The poly(amidoamine) dendrimer functionalized MMSNs was the best performing MMSNs that sequestered 54 mg U/ g adsorbent from the high salt water simulant, which is compared to 38 mg U/g from pH 3.5 AGW (i.e., phosphonate functionalized MMSNs) and 133 mg U/g from pH 9.6 AGW (i.e., poly(propylenimine) dendrimer MMSNs). Together, these adsorption capacities exceed or are competitive with other organo-functionalized high surface area adsorbents. In the future, the use of radiation-induced graft polymerization of acrylonitrile[41] onto high surface area mesoporous silica may be a synthesis route to produce even higher capacity sorbent materials for U sequestration from various aqueous media. Such effective sorbents have applications to environmental remediation, such as deployed in permeable reactive barrier or soil mixing system.

Additionally, these sorbents with extremely high adsorption capacities hold promise for selective mining U as an energy source from marine systems. Non-renewable fossil fuel reserves are unsustainable and unable to meet our future energy demands. Moreover, the production, refining and utilization of fossil fuels cause serious environmental pollution, with carbon dioxide emission recognized as a major source of greenhouse gasses. Nuclear energy generated through fission of U is viable technologically and economically for sustained based-load power production. If efficient and cost-competitive recovery technologies are developed for U mining from seawater, the vast reservoir of U resource in seawater can meet nuclear energy production at the present capacity for 72,000 years. Functionalized magnetic mesoporous silica nanoparticle adsorbent materials exhibited the adsorption capacity (~54 mg U/g adsorbent) of U removal from the HSW simulant. They may lead to feasible and economical technologies for U mining from seawater, which can potentially provide more sustainable U resources to nuclear power industry and mitigate environmental pollution caused by fossil fuel use. However, additional engineering measurements (e.g., long-term performance, the use of different real seawater, fouling) are needed to demonstrate that they were appropriate for this application.

■ ASSOCIATED CONTENT

Supporting Information

The Supporting Information is available free of charge on the ACS Publication website.

Additional details on synthesis of magnetite, synthesis and functionalization of MMSNs, structures of functionalized molecules (Figure S1), N_2 adsorption isotherm curves (Figure S2), small and high-angle XRD patterns (Figure S3), and TEM images (Figure S4) of functionalized MMSNs, ^{13}C CPMAS NMR spectra of functionalized MSNs (Figure S5), uranium phase

diagrams in the HSW simulant and AGW at the [U] = 2.5×10^{-5} M in equilibrium with atmospheric CO_2 (Figure S6), U adsorption coefficient values (K_d, mL/g) of non-functionalized and functionalized NMSNs in the HSW simulant (Figure S7), U L_3-edge XANES spectra of the functionalized MMSNs retrieved from the pH 3.5 and 9.6 AGW (Figure S8), U L_3-edge EXAFS spectra (Figure S9) and associated fitting parameters (Table S1) of the functionalized MMSNs retrieved from the pH 3.5 AGW, U L_3-edge EXAFS spectra (Figure S10) and associated fitting parameters (Table S2) of the functionalized MMSNs retrieved from the pH 9.6 AGW are given (PDF).

■ AUTHOR INFORMATION

Corresponding Author

*Phone: 803 725 7520. Fax: 803 725 7673. E-mail: Dien.Li@srs.gov.

Notes

The authors declare no competing financial interest.

■ ACKNOWLEDGEMENTS

This work was supported by the Laboratory Directed Research and Development (LDRD) program (Grant Nos.: LDRD-2014-00028 and LDRD-2015-00014) within the Savannah River National Laboratory (SRNL). Work was conducted at SRNL under the U.S. Department of Energy Contract DE-AC09-96SR18500. Dr. Seaman's participation was supported by the U. S. Department of Energy under Award Numbers DE-FC09-07SR22506 to the University of Georgia Research Foundation. Although Environmental Protection Agency (EPA) contributed to

this article, the research presented was not directly performed or funded by EPA and was not subjected to EPA's quality system requirements. Consequently, the views, interpretations, and conclusions expressed in this article are solely those of the authors and do not necessarily reflect or represent EPA's views or policies. MRCAT operations are supported by the Department of Energy and the MRCAT member institutions. This research used the resources of the Advanced Photon Source, an Office of Science User Facility operated for the U.S. Department of Energy (DOE) Office of Science by Argonne National Laboratory, and was supported by the U.S. DOE under Contract No. DE-AC02-06CH11357. In addition, Dr. Carter Abney from Oak Ridge National Laboratory (TN, USA) is gratefully acknowledged for his thoughtful discussion and kind assistance with U L_3-edge EXAFS data fittings.

■ REFERENCES

1. Strom, R. N.; Kaback, D. S., *Baseline Hydrogeologic Investigation: Aquifer Characterization Groundwater Geochemistry of the Savannah River Site and Vicinity (U); WSRC-RP-92-450*. Westinghouse Savannah River Company, Environmental Sciences Section: Aiken, SC, 1992.
2. Zachara, J. M.; Freshley, M. D.; Last, G. V.; Peterson, R. E.; Bjornstad, B. N., *Updated Conceptual Model for the 300 Area Uranium Groundwater Plume, PNNL-22048*. Pacific Northwest National Laboratory: Richland, Washington, 2012.
3. Lottermoser, B. G., *Mine Wastes: Characterization, Treatment and Environmental Impacts, Third Edition*. Springer: Heidelberg, Germany, 2010.
4. Wu, W. M.; Carley, J.; Luo, J.; Ginder-Vogel, M. A.; Cardenas, E.; Leigh, M. B.; Hwang, C. C.; Kelly, S. D.; Ruan, C. M.; Wu, L. Y.; Van Nostrand, J.; Gentry, T.; Lowe, K.; Mehlhorn, T.; Carroll, S.; Luo, W. S.; Fields, M. W.; Gu, B. H.; Watson, D.; Kemner, K. M.; Marsh, T.; Tiedje, J.; Zhou, J. Z.; Fendorf, S.; Kitanidis, P. K.; Jardine, P. M.; Criddle, C. S., In situ bioreduction of uranium (VI) to submicromolar levels and reoxidation by dissolved oxygen. *Environ. Sci. Technol.* 2007, *41*, (16), 5716-5723.
5. Gu, B.; Liang, L.; Dickey, M. J.; Yin, X.; Dai, S., Reductive precipitation of uranium(VI) by zero-valent iron. *Environ. Sci. Technol.* 1998, *32*, (21), 3366-3373.
6. Spycher, N. F.; Issarangkun, M.; Stewart, B. D.; Sengor, S. S.; Belding, E.; Ginn, T. R.; Peyton, B. M.; Sani, R. K., Biogenic uraninite precipitation and its reoxidation by iron(III) (hydr)oxides: A reaction modeling approach. *Geochim. Cosmochim. Acta* 2011, *75*, (16), 4426-4440.
7. Cerrato, J. M.; Ashner, M. N.; Alessi, D. S.; Lezama-Pacheco, J. S.; Bernier-Latmani, R.; Bargar, J. R.; Giammar, D. E., Relative reactivity of biogenic and chemogenic uraninite and biogenic noncrystalline U(IV). *Environ. Sci. Technol.* 2013, *47*, (17), 9756-9763.
8. Singh, G.; Sengor, S. S.; Bhalla, A.; Kumar, S.; De, J.; Stewart, B.; Spycher, N.; Ginn, T. M.; Peyton, B. M.; Sani, R. K., Reoxidation of biogenic reduced uranium: A challenge toward bioremediation. *Crit. Rev. Environ. Sci. Technol.* 2014, *44*, (4), 391-415.
9. Bardi, U., Extracting minerals from seawater: An energy analysis. *Sustainability* 2010, *2*, 980-992.
10. Kim, J.; Tsouris, C.; Mayes, R. T.; Oyola, Y.; Saito, T.; Janke, C. J.; Dai, S.; Schneider, E.; Sachde, D., Recovery of uranium from seawater: A review of current status and future research needs. *Sep. Sci. Technol.* 2013, *48*, (3), 367-387.
11. Tamada, M., Current status of technology for collection of uranium from seawater, http://www.physics.harvard.edu/~wilson/energypmp/2009_Tamada.pdf. 2009.
12. Hori, T.; Yamawaki, M.; Kanno, M., Uranium adsorption properties of hydrous titaniun-oxides in seawater. *J. Nucl. Sci. Technol.* 1987, *24*, (5), 377-384.
13. Das, S.; Oyola, Y.; Mayes, R. T.; Janke, C. J.; Kuo, L. J.; Gill, G.; Wood, J. R.; Dai, S., Extracting uranium from seawater: Promising AF series adsorbents. *Ind. Eng. Chem. Res.* 2016, *55*, (15), 4110-4117.
14. Gorka, J.; Mayes, R. T.; Baggetto, L.; Veith, G. M.; Dai, S., Sonochemical functionalization of mesoporous carbon for uranium extraction from seawater. *J. Mater. Chem. A* 2013, *1*, (9), 3016-3026.

15. Carboni, M.; Abney, C. W.; Taylor-Pashow, K. M. L.; Vivero-Escoto, J. L.; Lin, W. B., Uranium sorption with functionalized mesoporous carbon materials. *Ind. Eng. Chem. Res.* 2013, *52*, (43), 15187-15197.
16. Vivero-Escoto, J. L.; Carboni, M.; Abney, C. W.; deKrafft, K. E.; Lin, W. B., Organo-functionalized mesoporous silicas for efficient uranium extraction. *Microporous Mesoporous Mater.* 2013, *180*, 22-31.
17. Dudarko, O. A.; Gunathilake, C.; Wickramaratne, N. P.; Sliesarenko, V. V.; Zub, Y. L.; Gorka, J.; Dai, S.; Jaroniec, M., Synthesis of mesoporous silica-tethered phosphonic acid sorbents for uranium species from aqueous solutions. *Coll. Surf. A-Physicochem. Eng. Aspects* 2015, *482*, 1-8.
18. Gunathilake, C.; Gorka, J.; Dai, S.; Jaroniec, M., Amidoxime-modified mesoporous silica for uranium adsorption under seawater conditions. *J. Mater. Chem. A* 2015, *3*, (21), 11650-11659.
19. Tsezos, M.; Noh, S. H., Extraction of uranium from sea-water using biological origin adsorbents. *Can. J. Chem. Eng.* 1984, *62*, (4), 559-561.
20. Langmuir, D., Uranium solution-mineral equilibria at low temperatures with applications to sedimentary ore deposits. *Geochim. Cosmochim. Acta* 1978, *42*, 547-569.
21. Krupka, K. M.; Kaplan, D. I.; Whelan, G.; Serne, R. J.; Mattigod, S. V., *Understanding Variation in Partition Coefficient, Kd, Values. Volume II: Review of Geochemistry and Available Kd Values for Cadmium, Cesium, Chromium, Lead, Plutonium, Radon, Strontium, Thorium, Tritium (^{3}H), and Uranium," Rep. No. EPA 402-R-99-004*. USEPA: Washington, DC., 1999.
22. Grenthe, I.; Fuger, J.; Konings, R. J.; Lemire, R. J.; Muller, A. B.; Nguyen-Trung, C.; Wanner, H., *Chemical Thermodynamics of Uranium*. North-Holland: Amsterdam, 1992.
23. Zachara, J.; Brown, C.; Christensen, J.; Davis, J. A.; Dresel, E.; Liu, C.; Kelly, S.; McKinley, J.; Serne, J.; Um, W., *A Site-Wide Perspective on Uranium Geochemistry at the Hanford Site., PNNL-17031*. Pacific Northwest National Laboratory: Richland, WA., 2007.
24. Dong, W. M.; Brooks, S. C., Determination of the formation constants of ternary complexes of uranyl and carbonate with alkaline earth metals (Mg^{2+}, Ca^{2+}, Sr^{2+}, and Ba^{2+}) using anion exchange method. *Environ. Sci. Technol.* 2006, *40*, (15), 4689-4695.
25. Egodawatte, S.; Datt, A.; Burns, E. A.; Larsen, S. C., Chemical insight into the adsorption of chromium(III) on iron oxide/mesoporous silica nanocomposites. *Langmuir* 2015, *31*, (27), 7553-7562.
26. Li, D.; Egodawatte, S.; Kaplan, D. I.; Larsen, S. C.; Serkiz, S. M.; Seaman, J. C., Functionalized magnetic mesoporous silica nanoparticles for U removal from low and high pH groundwater. *J. Hazard. Mater.* 2016, *317*, 494-502.
27. Knezevic, N. Z.; Slowing, II; Lin, V. S. Y., Tuning the release of anticancer drugs from magnetic iron oxide/mesoporous silica core/shell nanoparticles. *Chempluschem* 2012, *77*, (1), 48-55.
28. Yuan, L. Y.; Liu, Y. L.; Shi, W. Q.; Li, Z. J.; Lan, J. H.; Feng, Y. X.; Zhao, Y. L.; Yuan, Y. L.; Chai, Z. F., A novel mesoporous material for uranium extraction, dihydroimidazole functionalized SBA-15. *J. Mater. Chem.* 2012, *22*, (33), 17019-17026.
29. Chen, J.; Qu, R. J.; Zhang, Y.; Sun, C. M.; Wang, C. H.; Ji, C. N.; Yin, P.; Chen, H.; Niu, Y. Z., Preparation of silica gel supported amidoxime adsorbents for selective adsorption of Hg(II) from aqueous solution. *Chem. Eng. J.* 2012, *209*, 235-244.

30. Wang, X. L.; Yuan, L. Y.; Wang, Y. F.; Li, Z. J.; Lan, J. H.; Liu, Y. L.; Feng, Y. X.; Zhao, Y. L.; Chai, Z. F.; Shi, W. Q., Mesoporous silica SBA-15 functionalized with phosphonate and amino groups for uranium uptake. *Sci. China-Chem.* 2012, *55*, (9), 1705-1711.
31. do Carmo, D. R.; Paim, L. L., Investigation about the copper adsorption on the chloropropylsilica gel surface modified with a nanostructured dendrimer DAB-Am-16: an analytical application for determination of copper in different samples. *Mate. Res.-Am. J. Mater.* 2013, *16*, (1), 164-172.
32. Saito, K.; Miyauchi, T., Chemical forms of uranium in artificial seawater. *J. Nucl. Sci. Technol.* 1982, *19*, (2), 145-150.
33. Segre, C. U.; Leyarovska, N. E.; Chapman, L. D.; Lavender, W. M.; Plag, P. W.; King, A. S.; Kropf, A. J.; Bunker, B. A.; Kemner, K. M.; Dutta, P.; Duran, R. S.; Kaduk, J., The MRCAT insertion device beamline at the Advanced Photon Source. In *Synchrotron Radiation Instrumentation: Eleventh US National Conference*, Pianetta, P.; Authur, J.; Brennan, S., Eds. American Institute of Physics: New York, 2000; Vol. 521, pp 419-422.
34. Calvin, S., *XAFS for Everyone*. CRC Press: Boca Raton, FL, 2013.
35. Ravel, B.; Newville, M., Athena, Artemis, Hephaestus: data analysis for X-ray absorption spectroscopy using IFEFFIT. *J. Synchrotron Radiat.* 2005, *12*, 537−541.
36. Kelly, S. D.; Kemner, K. M.; Fein, J. B.; Fowle, D. A.; Boyanov, M. I.; Bunker, B. A.; Yee, N., X-ray absorption fine structure determination of pH-dependent U-bacterial cell wall interactions. *Geochim. Cosmochim. Acta* 2002, *66*, (22), 3855-3871.
37. Vukovic, S.; Watson, L. A.; Kang, S. O.; Custelcean, R.; Hay, B. P., How amidoximate binds the uranyl cation. *Inorg. Chem.* 2012, *51*, (6), 3855-3859.
38. Morosin, B., Hydrogen uranyl phosphate tetrahydrate, a hydrogen-ion solid electrolyte. *Acta Crystallogr., Sect. B: Struct. Sci.* 1978, *34*, 3732−3734.
39. Demartin, F.; Gramaccioli, C. M.; Pilati, T., The importance of accurate crystal structure determination of uranium minerals. II. Soddyite $(UO_2)_2(SiO_4)\bullet 2H_2O$. *Acta Crystallogr. Sect. C* 1992, *48*, 1-4.
40. Pabalan, R. T.; Turner, D. R.; Bertetti, F. P.; J.D., P., Uranium(VI) sorption onto selected mineral surfaces - key geocjemical parameters. In *Adsorption of Metals by Geomedia*, Jenne, E. A., Ed. Academic Press: San Diego, USA, 1998.
41. Das, S.; Oyola, Y.; Mayes, R. T.; Janke, C. J.; Kuo, L. J.; Gill, G.; Wood, J. R.; Dai, S., Extracting uranium from seawater: Promising AF series adsorbents. *Ind. Eng. Chem. Res.* 2015.
42. Zhao, Y. G.; Li, J. X.; Zhang, S. W.; Wang, X. K., Amidoxime-functionalized magnetic mesoporous silica for selective sorption of U(VI). *Rsc Advances* 2014, *4*, (62), 32710-32717.
43. Alessi, D. S.; Lezama-Pacheco, J. S.; Stubbs, J. E.; Janousch, M.; Bargar, J. R.; Persson, P.; Bernier-Latmani, R., The product of microbial uranium reduction includes multiple species with U(IV)-phosphate coordination. *Geochim. Cosmochim. Acta* 2014, *131*, 115-127.
44. Bargar, J. R.; Reitmeyer, R.; Davis, J. A., Spectroscopic confirmation of uranium(VI)-carbonato adsorption complexes on hematite. *Environ. Sci. Technol. 1*999, *33*, (14), 2481-2484.
45. Fischer, H.; Luster, J.; Gehring, A. U., EPR evidence for maghemitization of magnetite in a tropical soil. *Geophys. J. Internat.* 2007, *169*, (3), 909-916.
46. Krzyminiewski, R.; Kubiak, T.; Dobosz, B.; Schroeder, G.; Kurczewska, J., EPR spectroscopy and imaging of TEMPO-labeled magnetite nanoparticles. *Cur. Appl. Phys.* 2014, *14*, (5), 798-804.

47. Alessi, A.; Agnello, S.; Buscarino, G.; Pan, Y.; Mashkovtsev, R. I., EPR on radiation-induced defects in SiO_2. In *Applications of EPR in Radiation Research*, Lund, A.; Shiotani, M., Eds. Springer: 2014; pp 255-298.
48. Sadlo, J.; Bugaj, A.; Strzelczak, G.; Sterniczuk, M.; Jaegermann, Z., Multifrequency EPR study on radiation induced centers in calcium carbonates labeled with C-13. *Nukleonika* 2015, *60*, (3), 429-434.
49. Vorona, I. P.; Nosenko, V. V.; Baran, N. P.; Ishchenko, S. S.; Lemishko, S. V.; Zatovsky, I. V.; Strutynska, N. Y., EPR study of radiation-induced defects in carbonate-containing hydroxyapatite annealed at high temperature. *Rad. Measurements* 2016, *87*, 49-55.
50. Pan, Y. M.; Nilges, M. J., Electron Paramagnetic Resonance Spectroscopy: Basic Principles, Experimental Techniques and Applications to Earth and Planetary Sciences. In *Spectroscopic Methods in Mineralology and Materials Sciences*, Henderson, G. S.; Neuville, D. R.; Downs, R. T., Eds. 2014; Vol. 78, pp 655-690.
51. Elzinga, E. J.; Tait, C. D.; Reeder, R. J.; Rector, K. D.; Donohoe, R. J.; Morris, D. E., Spectroscopic investigation of U(VI) sorption at the calcite-water interface. *Geochim. Cosmochim. Acta* 2004, *68*, (11), 2437-2448.
52. Fuller, C. C.; Bargar, J. R.; Davis, J. A., Molecular-scale characterization of uranium sorption by bone apatite materials for a permeable reactive barrier demonstration. *Environ. Sci. Technol.* 2003, *37*, (20), 4642-4649.
53. Singer, D. M.; Maher, K.; Brown, G. E., Uranyl-chlorite sorption/desorption: Evaluation of different U(VI) sequestration processes. *Geochim. Cosmochim. Acta* 2009, *73*, (20), 5989-6007.
54. Singer, D. M.; Guo, H.; Davis, J. A., U(VI) and Sr(II) batch sorption and diffusion kinetics into mesoporous silica (MCM-41). *Chem. Geol.* 2014, *390*, 152-163.
55. Abney, C. W.; Mayes, R. T.; Piechowicz, M.; Lin, Z.; Bryantsev, V. S.; Veith, G. M.; Dai, S.; Lin, W., XAFS investigation of polyamidoxime-bound uranyl contests the paradigm from small molecule studies. *Energy Environ. Sci.* 2016, *9*, (2), 448-453.
56. Tian, G. X.; Teat, S. J.; Rao, L. F., Thermodynamic studies of U(VI) complexation with glutardiamidoxime for sequestration of uranium from seawater. *Dalton Trans.* 2013, *42*, (16), 5690-5696.
57. Sun, X. Q.; Tian, G. X.; Xu, C.; Rao, L. F.; Vukovic, S.; Kang, S. O.; Hay, B. P., Quantifying the binding strength of U(VI) with phthalimidedioxime in comparison with glutarimidedioxime. *Dalton Trans.* 2014, *43*, (2), 551-557.
58. Burns, P. C., U^{6+} minerals and inorganic compounds: Insights into an expanded structural hierarchy of crystal structures. *Can. Mineral.* 2005, *43*, 1839-1894.
59. Tian, G. X.; Teat, S. J.; Zhang, Z. Y.; Rao, L. F., Sequestering uranium from seawater: binding strength and modes of uranyl complexes with glutarimidedioxime. *Dalton Trans.* 2012, *41*, (38), 11579-11586.
60. Sylwester, E. R.; Hudson, E. A.; Allen, P. G., The structure of uranium (VI) sorption complexes on silica, alumina, and montmorillonite. *Geochim. Cosmochim. Acta* 2000, *64*, (14), 2431-2438.
61. Catalano, J. G.; Brown, G. E., Analysis of uranyl-bearing phases by EXAFS spectroscopy: Interferences, multiple scattering, accuracy of structural parameters, and spectral differences. *Am. Mineral.* 2004, *89*, (7), 1004-1021.

710 Table 1. Saturated Adsorption Capacity of Functionalized MMSNs for Uranium Removal from
711 HSW simulant, pH 3.5 and 9.6 AGW
712

Samples	HSW simulant		pH 3.5 AGW*		pH 9.6 AGW*	
	q_{max} (mg/g)	R^2	q_{max} (mg/g)	R^2	q_{max} (mg/g)	R^2
MMSNs-DIM	34.1 ± 1.86	0.992	24.9 ± 3.0	0.957	109.9 ± 8.5	0.982
MMSNs-AD	45.6 ± 8.27	0.912	30.6 ± 4.9	0.951	125.0 ± 10.9	0.980
MMSNs-PP	45.3 ± 4.92	0.967	37.5 ± 0.8	0.998	55.0 ± 5.1	0.976
MMSNs-PPA	51.6 ± 7.71	0.918	20.6 ± 2.7	0.952	108.7 ± 3.6	0.997
MMSNs-PPI	52.1 ± 4.88	0.967	9.5 ± 1.0	0.965	133.3 ± 6.2	0.933
MMSNs-PM	53.8 ± 10.4	0.868			29.4 ± 0.4	0.999
* Data from pH 3.5 and pH 9.6 AGW were previously reported, and are included here for the purpose of comparison. It is noted that organic functionalization on MMSNs would minimize the potential dissolution of MMSNs in the pH 9.6 AGW.						

713
714
715

716 Table 2. The Fit Parameters of U L_3-edge EAXFS Data of Functionalized MMSNs After
717 Exposure to U in the HSW Simulant
718

Samples[a]	Scattering paths	Interatomic distance (Å)[b]	Coordination number[c]	Debye–Waller factor, σ^2 (Å^2)[b]	E_0	R-factor
MMSNs-DIM	U-O_{ax}	1.80 (1)	2	0.003 (1)	6.4 ± 2.4	0.0024
	U-O_{eq}	2.25 (5)	3.8	0.008 (4)		
	U-N[d]	2.34 (5)	1.2	0.008 (4)		
	U-Si	3.13 (2)	0.4	0.001 (7)		
MMSNs-AD	U-O_{ax}	1.80 (1)	2	0.002 (1)	6.6 ± 2.5	0.0029
	U-O_{eq}	2.26 (5)	3.6	0.008 (4)		
	U-N	2.34 (5)	1.4	0.008 (4)		
	U-Si	3.14 (3)	0.4	0.002 (9)		
MMSNs-PP	U-O_{ax}	1.81 (1)	2	0.003 (1)	6.8 ± 4.0	0.0030
	U-O_{eq}	2.26 (2)	5.1	0.008 (3)		
	U-P	3.56 (3)	0.9	0.02 (3)		
	U-Si	3.13 (4)	0.6	0.003 (5)		
MMSNs-PPA	U-O_{ax}	1.80 (1)	2	0.003 (1)	7.3 ± 2.1	0.0028
	U-O_{eq}	2.26 (1)	4.1	0.008 (1)		
	U-N	2.34 (1)	0.9	0.008 (1)		
	U-Si	3.13 (2)	0.7	0.003 (5)		
MMSNs-PPI	U-O_{ax}	1.80 (1)	2	0.003 (1)	7.3 ± 2.3	0.0027
	U-O_{eq}	2.25 (4)	3.4	0.007 (3)		
	U-N	2.34 (4)	1.6	0.007 (3)		
	U-Si	3.13 (3)	0.6	0.004 (8)		
MMSNs-PM	U-O_{ax}	1.80 (1)	2	0.003 (1)	6.6 ± 2.1	0.0028
	U-O_{eq}	2.25 (4)	4.3	0.008 (4)		
	U-N	2.34 (4)	0.7	0.008 (4)		
	U-Si	3.12 (2)	0.4	0.002 (3)		

[a] Amplitude was set at 1 for data fitting of all samples.

[b] The uncertainty as calculated by Artemis are listed in parentheses, representing the errors in the last digit.

[c] Coordination number of the axial uranyl oxygen atoms was set at 2. The errors for the other coordination numbers are ±30%.

[d] Total coordination numbers of the equatorial uranyl oxygen and nitrogen atoms were set at 5, and variations in interatomic distance and Debye–Waller factor of the U-O_{eq} and U-N paths were set identical.

719
720

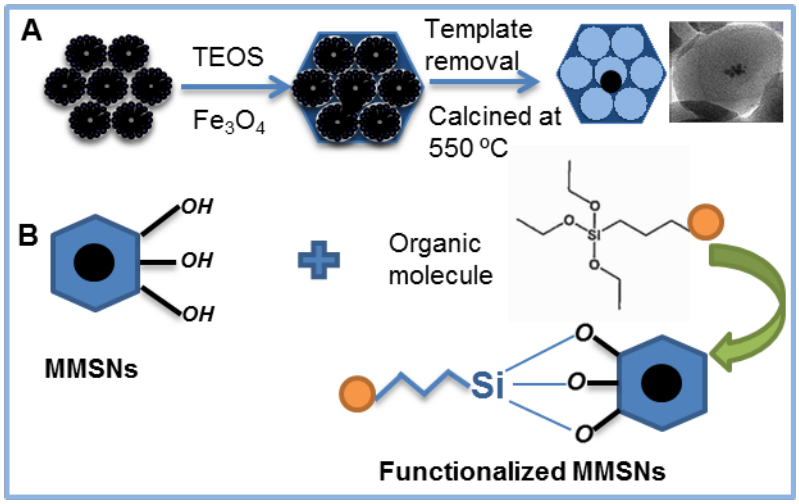

Figure 1. Schemes for the synthesis (A) and functionalization (B) of magnetic mesoporous silica nanoparticles (MMSNs).

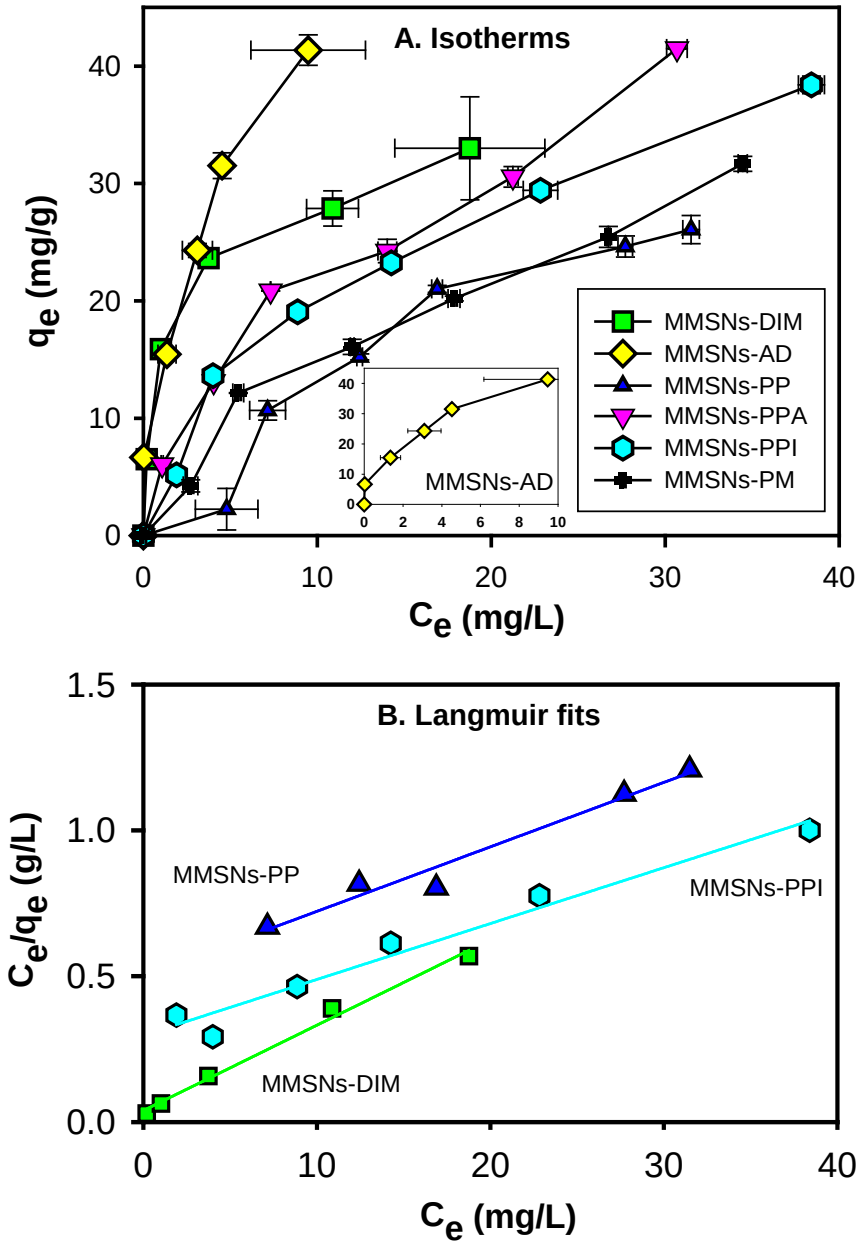

Figure 2. Adsorption isotherms for U on the dihydroimidazole (DIM), polyacryloamidoxime (AD), phosphonate (PP), phosphonate-amino (PPA), poly(propylenimine) dendrimer (PPI), and poly(amidoamine) dendrimer (PM) functionalized MMSNs in the HSW simulant (A) and representative Langmuir fits for MMSNs-DIM, MMSNs-PP, and MMSNs-PPI (B). The inset in Figure 2A shows the MMSNs-AD data in an expanded scale. The lines in Figure 2B visibly depicted the Langmuir fits to the experimental data.

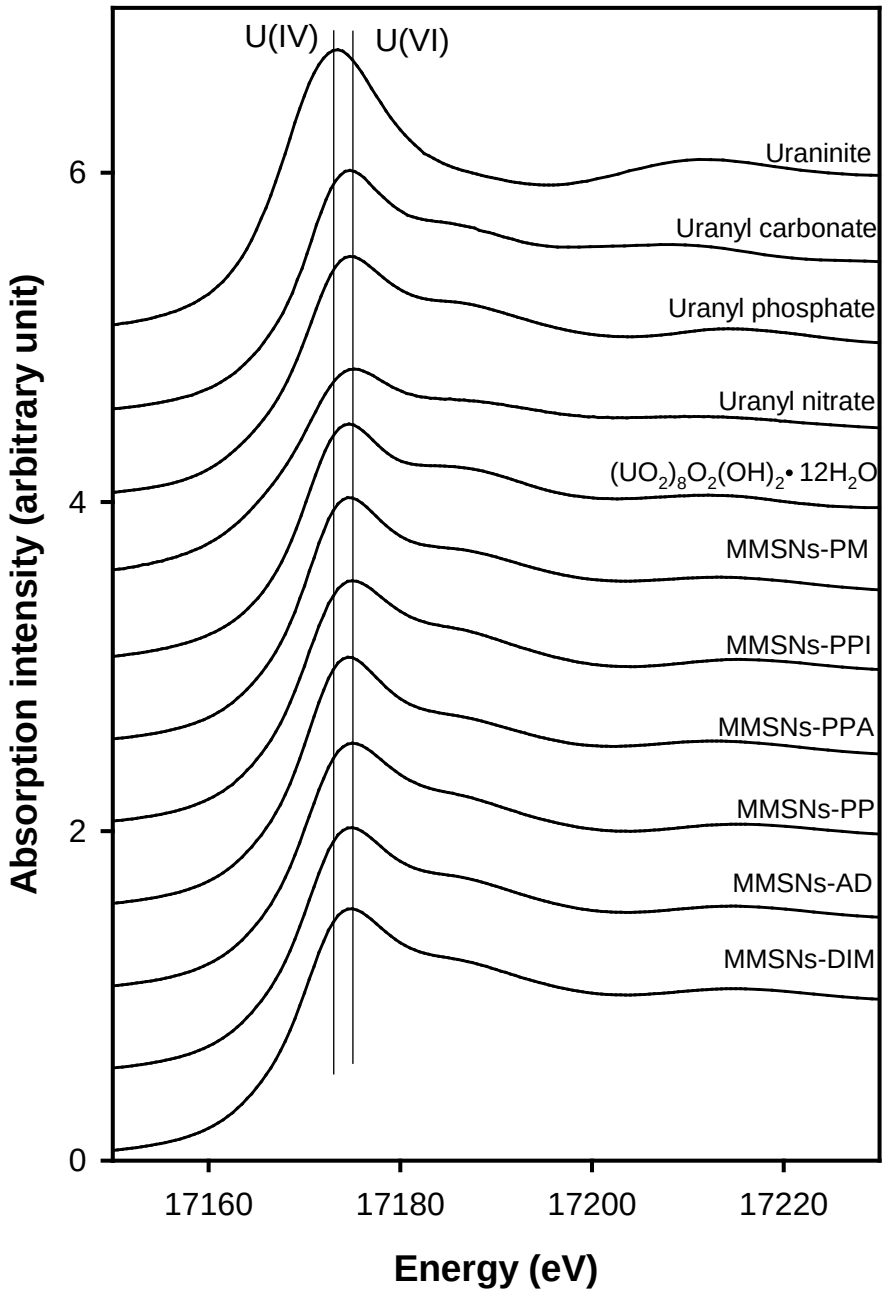

Figure 3. U L_3-edge XANES spectra of functionalized MMSNs with U adsorption from the HSW simulant. Several model compounds were included for comparison. Lines denote the peak of the white line for U(IV) and U(VI) controls, affirming the U(VI) species is bound by MMSN materials. The spectrum of UO_2 (uraninite) standard was collected soon after it was purchased from Alfar Aesar (Ward Hill, MA) and its surface oxidation was minimal.

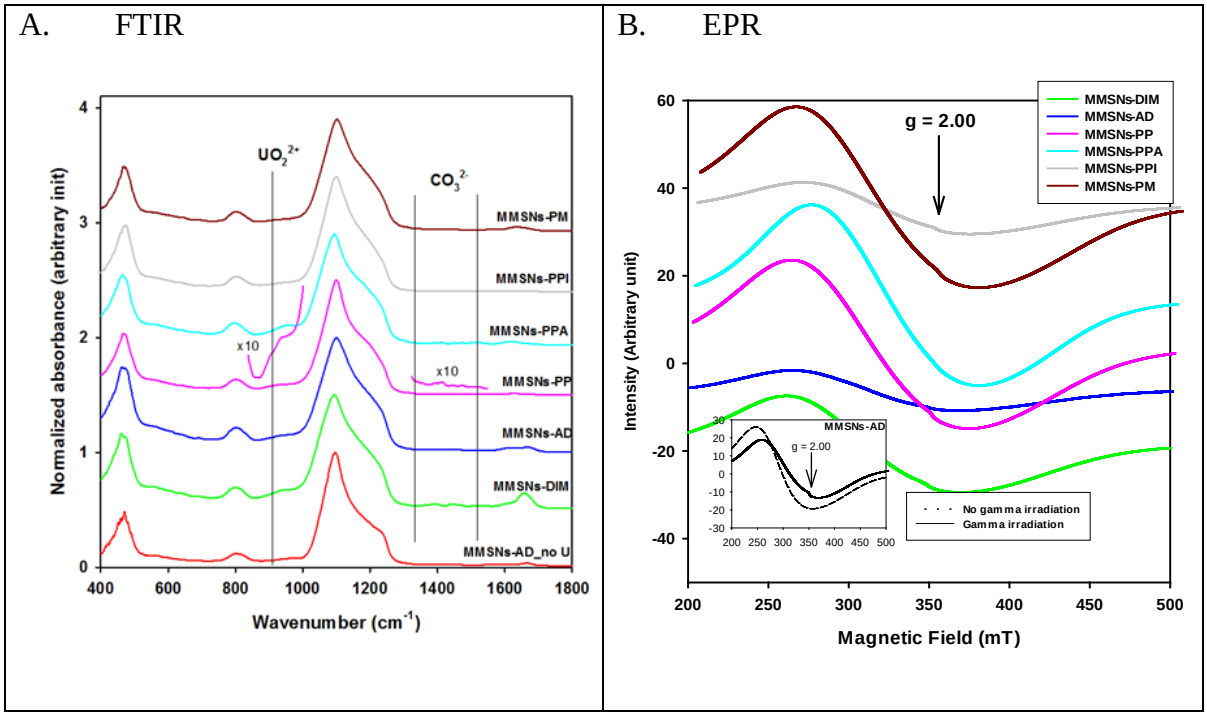

Figure 4. FTIR (A) and powder EPR (B) spectra of the dihydroimidazole (DIM), polyacryloamidoxime (AD), phosphonate (PP), phosphonate-amino (PPA), poly(propylenimine) dendrimer (PPI), and poly(amidoamine) dendrimer (PM) functionalized MMSNs samples with exposed to U in the HSW simulant. The FTIR spectrum of MMSNs-PP was amplified by 10 times in the ranges of 840-1000 cm^{-1} and 1320-1550 cm^{-1}. While the signal for UO_2^{2+} was clearly observed, the signals for CO_3^{2-} in the range of 1320-1550 cm^{-1} were within the noise level. The EPR spectra were measured for the gamma-ray-irradiated samples at microwave frequencies of ~9.73 GHz and a microwave power of 6.35 mW, illustrating the broad signal centered at g_{eff} = ~2.20. The EPR spectra of polyacryloamidoxime (AD) functionalized MMSNs without U exposure before and after gamma irradiation were also included in the inset of Figure 4B, where a weak resonance signal at g_{eff} = ~2.00 (marked by an arrow) was present in the irradiated MMSNs-AD.

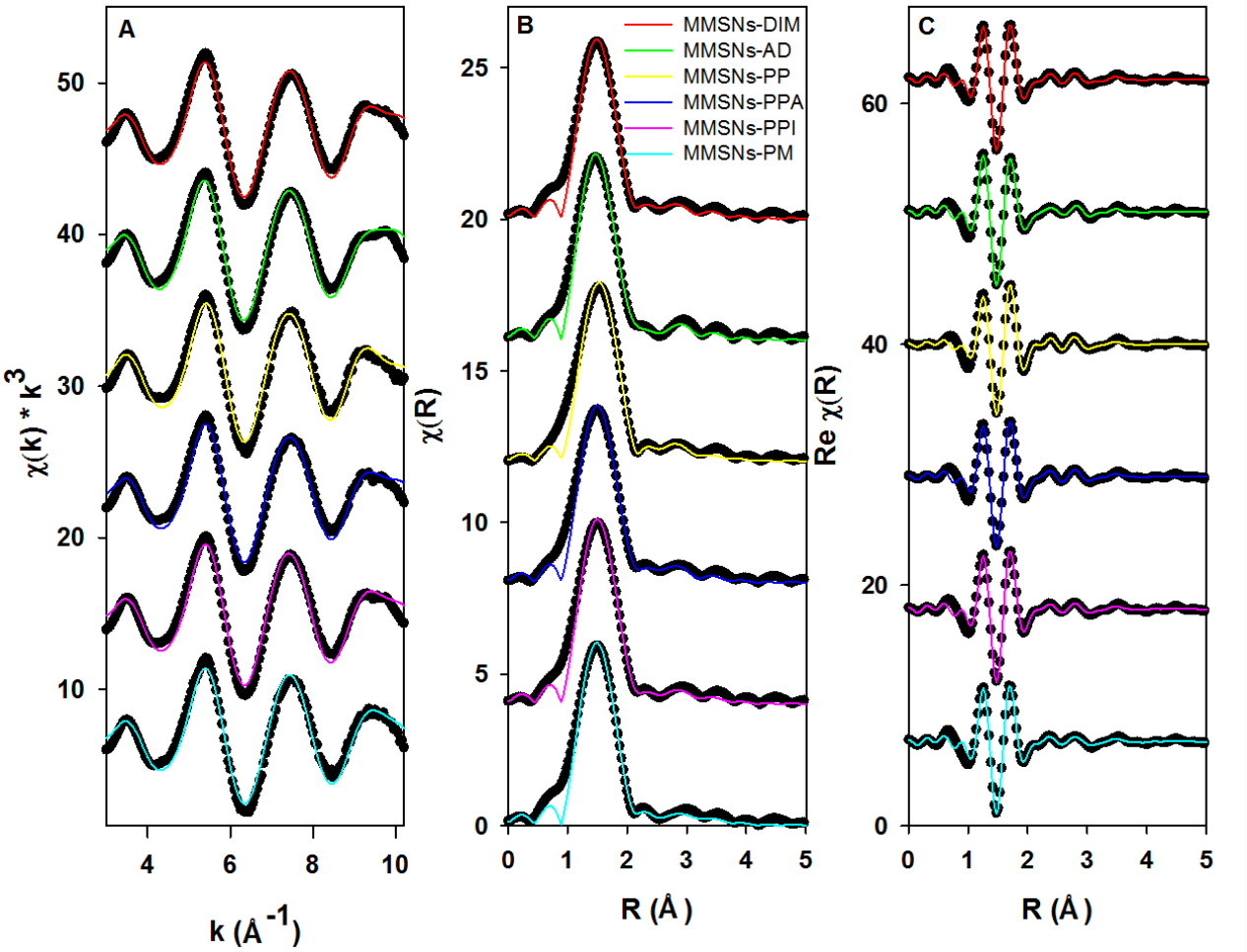

Figure 5. U L_3-edge EXAFS spectra in k-space (A), Fourier transform plots in magnitude (B) and in the real space component (C) of the functionalized MMSNs with U adsorption from the HSW simulant. Experimental data are shown in solid circles, and EXAFS fits are shown in color lines.

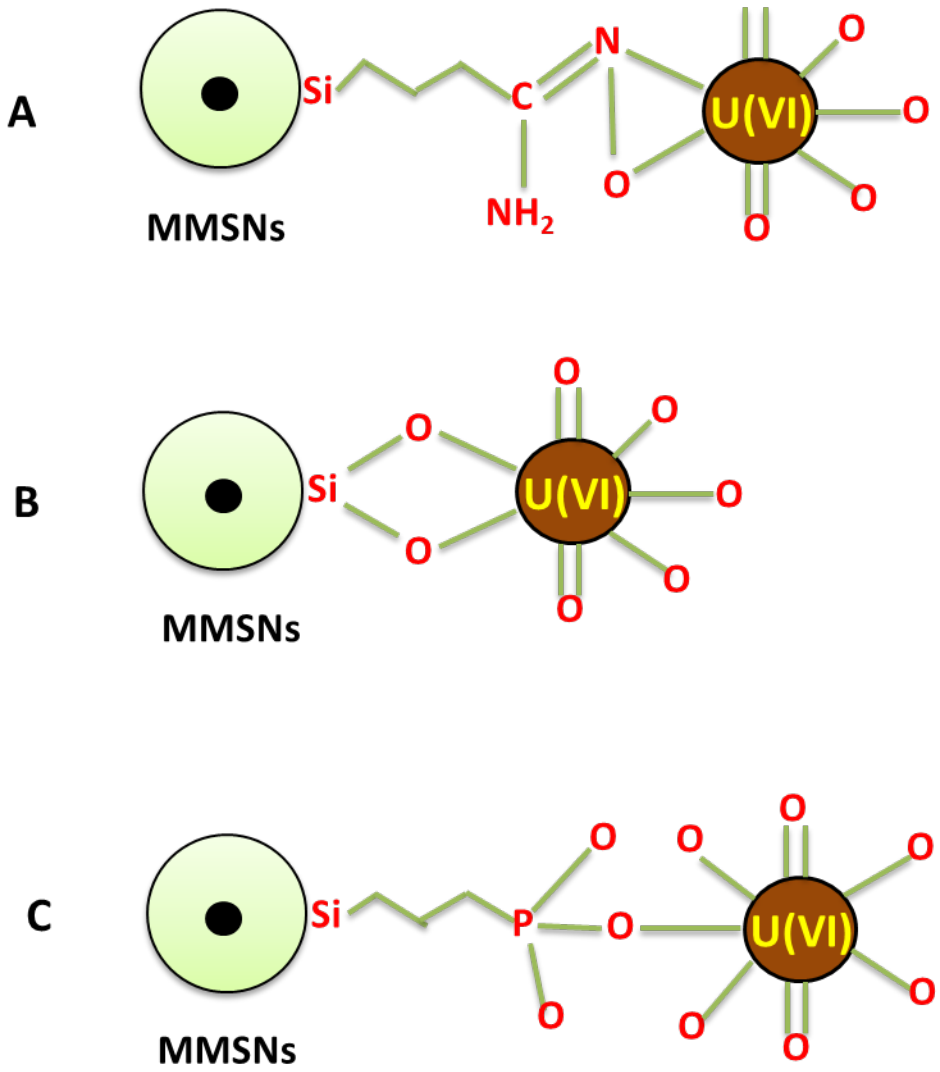

772
773
774 Figure 6. Typical chemical binding sites of uranyl species onto functionalized MMSNs in the
775 HSW simulant. A. Nitrogen ligands as η^2-bound motif, B. Silanol bound, C. Phosphonate
776 ligand as a monodentate.
777
778
779